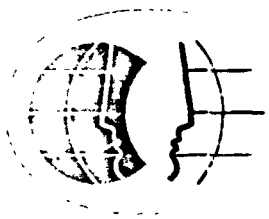

(NASA-CR-144311) ZERO-GRAVITY GROWTH OF NaF-NaCl EUTECTICS IN THE NASA SKYLAB PROGRAM Final Report (California Univ.) 67 p HC $4.50 CSCL 11D

N76-24289

Unclas

G3/12 28263

UCLA-ENG-7609
JANUARY 1976

ZERO-GRAVITY GROWTH OF Na F-Na Cl EUTECTICS IN THE NASA SKYLAB PROGRAM

A.S. YUE
F.G. ALLEN
J.G. YU

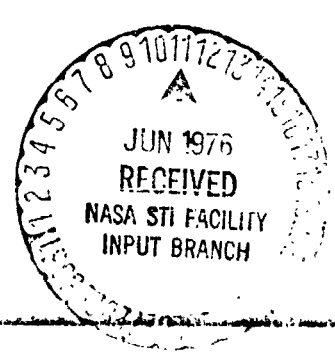

SECURITY CLASSIFICATION OF THIS PAGE (When Data Entered)

REPORT DOCUMENTATION PAGE		READ INSTRUCTIONS BEFORE COMPLETING FORM
1. REPORT NUMBER UCLA-ENG-7609	2. GOVT ACCESSION NO.	3. RECIPIENT'S CATALOG NUMBER
4. TITLE (and Subtitle) ZERO-GRAVITY GROWTH OF NaF-NaCl EUTECTICS IN THE NASA SKYLAB PROGRAM		5. TYPE OF REPORT & PERIOD COVERED FINAL 6. PERFORMING ORG. REPORT NUMBER
7. AUTHOR(s) A.S. Yue F.G. Allen J.G. Yu		8. CONTRACT OR GRANT NUMBER(s) NAS-8-28310
9. PERFORMING ORGANIZATION NAME AND ADDRESS School of Engineering and Applied Science University of California Los Angeles, CA 90024		10. PROGRAM ELEMENT, PROJECT, TASK AREA & WORK UNIT NUMBERS
11. CONTROLLING OFFICE NAME AND ADDRESS George C. Marshall Space Flight Center Huntsville, Alabama 35812		12. REPORT DATE January 1976 13. NUMBER OF PAGES 65
14. MONITORING AGENCY NAME & ADDRESS (if different from Controlling Office) Office of Naval Research 1030 East Green Street Pasadena, Calif. 91106		15. SECURITY CLASS. (of this report) Unclassified 15a. DECLASSIFICATION/DOWNGRADING SCHEDULE

16. DISTRIBUTION STATEMENT (of this Report)

17. DISTRIBUTION STATEMENT (of the abstract entered in Block 20, if different from Report)

18. SUPPLEMENTARY NOTES

19. KEY WORDS (Continue on reverse side if necessary and identify by block number)

Zero-gravity, eutectic growth, eutectic fibers, optical fibers, sodium chloride, sodium fluoride, skylab, NASA, infra-red polarizer

20. ABSTRACT (Continue on reverse side if necessary and identify by block number)

Continuous and discontinuous NaF fibers, embedded in a NaCl matrix, have been produced in space and on earth, respectively. The production of continuous fibers in a eutectic mixture was attributed to the absence of convection current in the liquid during solidification in space. Image transmission and optical transmittance measurements of transverse sections of the space-grown and earth-grown ingots were made with a light microscope and a spectrometer. It was found that better optical properties were obtained from samples grown

over

DD FORM 1 JAN 73 1473 EDITION OF 1 NOV 65 IS OBSOLETE
S/N 0102-LF 014-6601

SECURITY CLASSIFICATION OF THIS PAGE (When Data Entered)

in space. This was attributed to a better alignment of NaF fibers along the ingot axis.

A new concept is advanced to explain the phenomenon of transmittance versus far infrared wavelength of the directionally solidified NaCl-NaF eutectic in terms of the two-dimensional Bragg Scattering and the polarization effect of Rayleigh scattering. This concept can be applied to other eutectic systems as long as the index of refraction of the matrix over a range of wavelengths is known. Experimental data are in excellent agreement with the theoretical prediction.

UCLA-ENG-7609
January 1976

ZERO-GRAVITY GROWTH OF NaF-NaCℓ EUTECTICS IN THE NASA SKYLAB PROGRAM

A.S. YUE
F.G. ALLEN
J.G. YU

FINAL REPORT

NASA GRANT NAS-8-28310

School of Engineering and Applied Science
University of California
Los Angeles, California

ABSTRACT

Continuous and discontinuous NaF fibers, mbedded in a NaCl matrix, have been produced in space and on earth, respectively. The production of continuous fibers in a eutectic mixture was attributed to the absence of convection current in the liquid during solidification in space. Image transmission and optical transmittance measurements of transverse sections of the space-grown and earth-grown ingots were made with a light microscope and a spectrometer. It was found that better optical properties were obtained from samples grown in space. This was attributed to a better alignment of NaF fibers along the ingot axis.

A new concept is advanced to explain the phenomenon of transmittance versus far infrared wavelength of the directionally solidified NaCl-NaF eutectic in terms of the two-dimensional Bragg Scattering and the polarization effect of Rayleigh scattering. This concept can be applied to other eutectic systems as long as the index of refraction of the matrix over a range of wavelengths is known. Experimental data are in excellent agreement with the theoretical prediction.

CONTENTS

FIGURE CAPTIONS

FIGURE CAPTIONS (Continued)

FIGURE CAPTIONS (Continued)

PRECEDING PAGE BLANK NOT FILMED.

Section 1

INTRODUCTION

When certain binary eutectic mixtures solidify, one of the two phases can form fibers or platelets in a matrix of the second phase. For example, when a eutectic liquid of NaCl and NaF solidifies, fibers of NaF form in a matrix of NaCl.

Fiberlike and platelike eutectics produced on Earth are limited in perfection by the presence of a banded structure, [1,2] discontinuity, [3] and faults [4,5] due, at least in part, to vibration and convection currents in the melt during solidification. The presence of these defects renders the solid-state eutectic devices inefficient and useless.[6] However, if the solidification process is performed in a space environment, where there is no vibration and convection current in the melt, there is reason to hope that fault-free, continuous and perfect platelike and fiberlike eutectic microstructures can be produced. Thus, the electrical, thermomagnetic, and superconducting chracteristics of such eutectics will be strongly anisotropic, and this will make possible various exciting device applications.

Section 2

OBJECTIVES

The objectives of this project were: (1) to prepare, in a space experiment, fiberlike NaF-NaCl eutectic with continuous fibers embedded in the matrix. This eutectic cannot be produced on Earth due to the presence of convection currents and vibration in the melt during solidification; (2) to extract a few fibers from a Skylab-grown NaCl-NaF eutectic ingot and also from Earth-grown ingots, and to determine whether the extracted fibers were continuous or discontinuous; (3) to sketch a hypothetical advancing solid-liquid NaCl-NaF eutectic interface; (4) to calculate the interfiber spacing of the NaF fibers; and (5) to measure transmittance versus wavelength curves of Skylab-grown, and Earth-grown ingots, both along and perpendicular to the fiber axes.

Section 3

EXPERIMENTAL PROCEDURE

NaCl-21 wt% NaF eutectic ingots were prepared from 99.96% NaCl and 99.7% NaF, obtained from Research Organic-Inorganic Chemical Corporation, Sun Valley, California. The salt ingots were melted and solidified in an induction furnace under an argon atmosphere. After solidification, each ingot was machined to the shape and dimensions as depicted in Figure 1, labeled as Sample.

To hold the salt ingot, a graphite crucible was machined from a high purity graphite rod 1/2 in. in diameter and 12 in. long, obtained from Ultra Carbon Corporation, Bay City, Michigan to the dimensions of 4 in. in length, 0.350 in. O.D., and 0.310 in. I.D. Since graphite is a very fragile material, a special method was employed to machine the crucibles. Starting with a 0.5 in. rod mounted in a lathe, the 0.310 in. hole was drilled so as to be concentric with the graphite rod. Then a 0.31 in. brass rod was inserted into the 0.310 in. hole to give the graphite tube support while the outer diameter was machined from 0.5 in. to 0.35 in. in diameter. The graphite crucibles were cut to 4.375 in. in length and then calcined in vacuum at 950 deg. C for 25 hours.

The salt ingot-graphite crucible assembly was then loaded into a 304 stainless steel container of dimensions shown in Figure 1. The steel container was made from 0.375 in. O.D. and 0.355 in. I.D. stainless steel tubing obtained from Tube Sales Co., Los Angeles, California, with a stainless steel plug heliarc-welded to one end of the tube. After loading the ingot-crucible assembly, the inner wall of the stainless steel container was coated with a graphite paste where the salt ingot is exposed to the container. Then a calcined graphite disk (0.010 in. thick) was placed over the end of the ingot. The graphite paste and disk were employed to prevent a reaction between the container and the salt when the salt was later remelted and resolidified. The

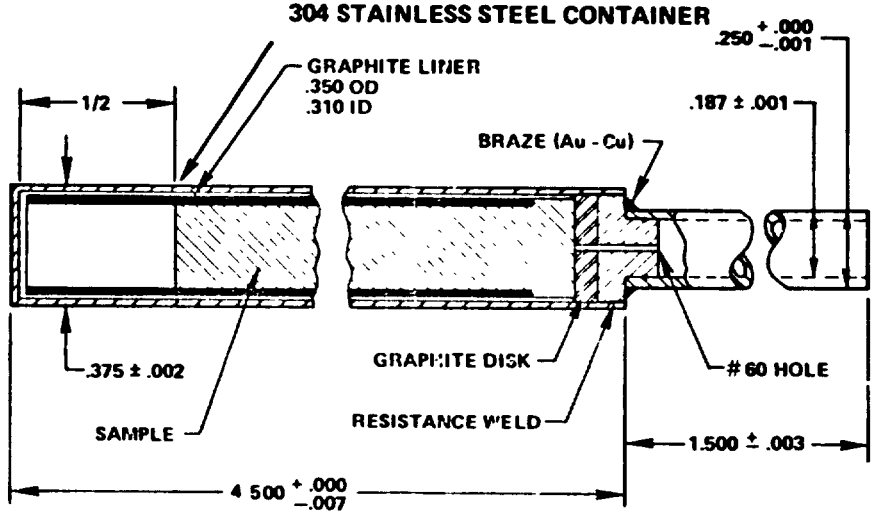

Figure 1. Sketch of an ampoule.

The solidification experiment was carried out in a multipurpose electric furnace[7] at a freezing rate of 0.6°C/min. and a temperature gradient of 50°C/cm. The procedure for conducting the experiment is automatic.

container was then sealed by heliarc welding a cap, with a #60 vent hole as shown in Figure 1, in place.

There were three groups of samples involved. All were prepared initially at UCLA. The first set was retained at UCLA for later comparison, (group A). The second was sent to Westinghouse Laboratories to be regrown in a proto-type furnace for comparison with the space grown samples, (group B). The third group of three samples went from UCLA to the Skylab for growth in space, (group C).

The resolidification experiment in Skylab 3 was carried out in a multi-purpose electric furnace.[7] One-half inch of the eutectic sample in this experiment adjacent to the graphite disk was left unmelted and the remaining portion of the sample was melted and resolidified unidirectionally toward the empty space of the ampoule as indicated in Figure 1. The solidification rate was 0.6°C/min and the temperature gradient was 50°C/cm.

Section 4

RESULTS

The experimental results are presented in five parts. The first part concerns the macro- and microstructures of the samples that were grown in Skylab 3 and on Earth. The second part concerns the extraction of continuous NaF fibers embedded in a NaCl matrix. The third part deals with the shape of the advancing solid-liquid interface of the Skylab-grown ingot. The fourth part is to calculate the interfiber spacing of the NaF fibers of the Skylab-grown NaCl-NaF eutectic. The fifth part concerns the image transmission of the NaCl-NaF eutectic, and the sixth part, the optical transmittance.

4.1 Macro- and Microstructures

After the space experiment the three ampoules were hand-carried to us by Mr. Williams of NASA and were given three identity numbers (M564-6, M564-10, and M564-11). Radiography for voids was carried out at NASA, Huntsville. Figure 2b is a radiograph of the three large cylindrical cartridges* containing the three samples and Figure 2a is a radiograph of the three ampoules, after they had been removed from the cartridges. In both figures, voids are present in all three samples. Sample #10 of Figure 2a shows the presence of a disconnection which apparently occurred when the ampoule was removed from the cartridge.

Figure 3 is a macro-photograph showing the appearance of the three ampoules after the space experiment. The surfaces of the stainless steel cylinders and the copper tubing were in perfect condition. Remelting of the silver solder was not detected in the joint binding the stainless steel cylinder and copper tubing together.

---

*Note brass plugs at one end of cartridge and stainless steel tubes (about 1" dia) at the other.

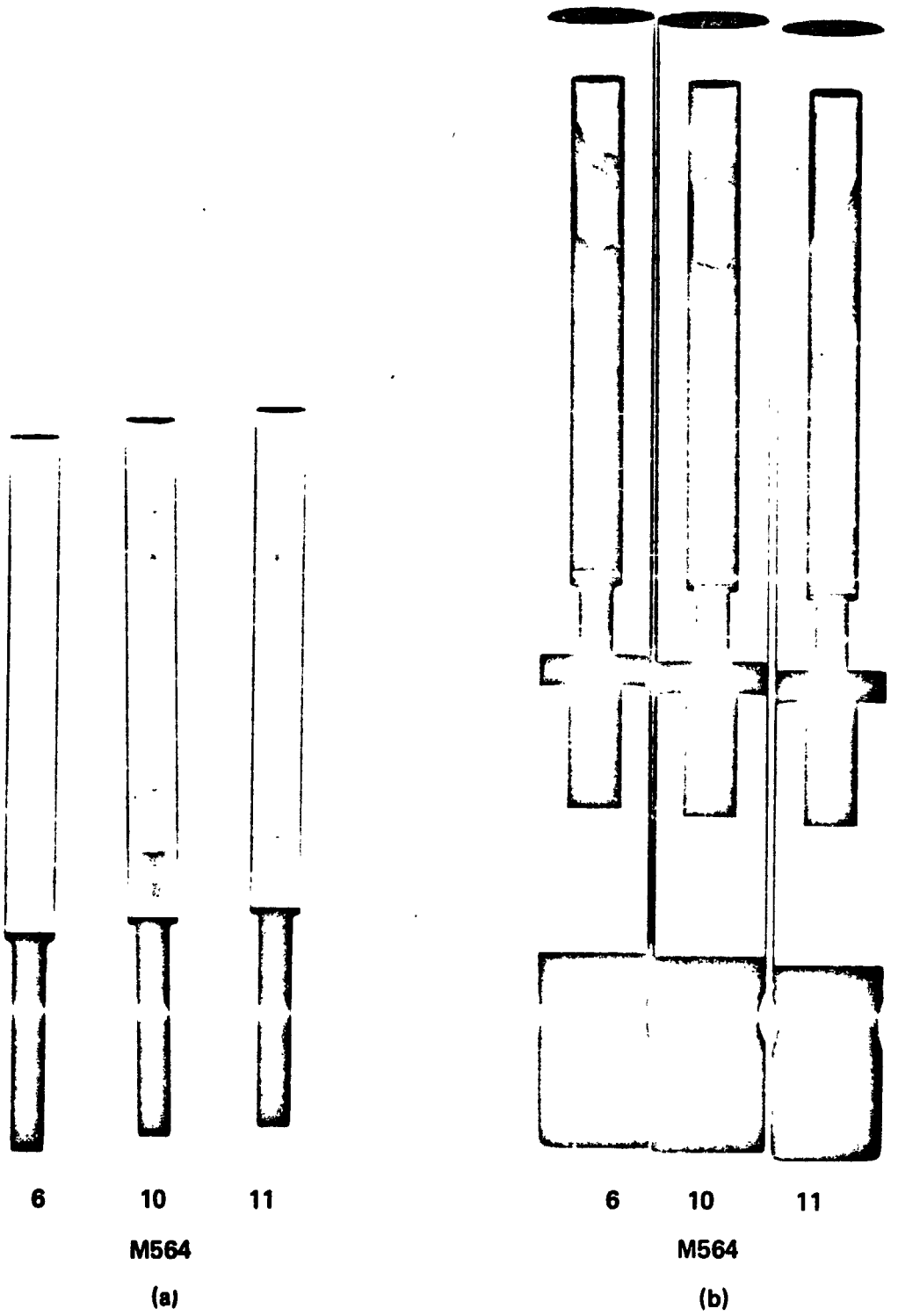

Figure 2. Space-Grown Samples.
(a) Radiograph of three ampoules after removal from cartridges.
(b) Radiograph of three cartridges containing ampoules.

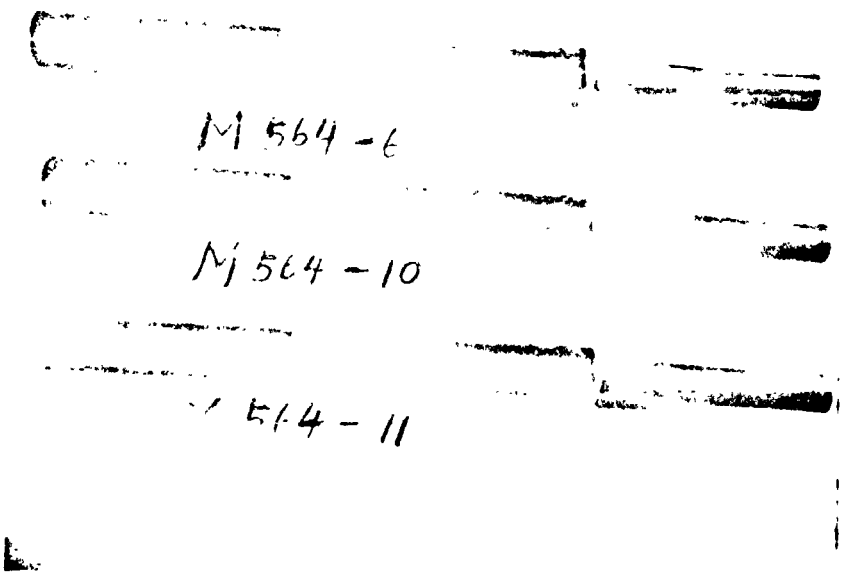

Figure 3. Photomacrograph of the Three Skylab Ampoules. X0.8

Figure 4 is a macro-photograph of the three skylab-grown samples taken out of the ampoules by grinding off the welded ends of each stainless steel cylinder. Careful inspection of the surface of the samples revealed no reaction between the NaCl-NaF eutectic and the graphite container. In sample #10, two transverse fractures surfaces occurred, both at the head and tail portions of the sample as revealed in Figure 4. However, the fracture, which occurred after the re-solidification, did not interrupt the growth pattern of the sample.

Figure 5 is a macro-photograph of the solidified sample (number 6), showing the geometry of the meltback interface, columnar grains of the solidified portion of the sample (on the right of the interface), and the unmelted portion of the sample (on the left of the interface). An enlarged portion of the solid-liquid interface is given in Figure 6 which shows the beginning of the solidification process. The NaF fibers here grew in a direction perpendicular to the intended direction. This indicates that the direction of heat extraction during the onset of solidification was not parallel to the growth direction as intended. However, in a distance not far away from the initial solid-liquid interface (about 0.08 cm), the NaF fibers began to align toward the growth direction. Figure 7 is a representative photomicrograph of a longitudinal section of sample #6 showing the long continuous fibers. A representative photomicrograph of a transverse section of a sample is shown in Figure 8 which reveals the shapes of the fibers which are preferentially rectangular with rounded or angular ends. A scanning electron photomicrograph showing the shapes of NaF fibers grown on Earth, (from group B), is given in Figure 9a, which is the perspective view of the rectangular NaF fibers, protruding from the continuous NaCl matrix. Notice that the fibers are not parallel to one another. Figure 9b shows a corresponding SEM view of the Skylab-grown ingot, showing that all the NaF fibers are aligned in one

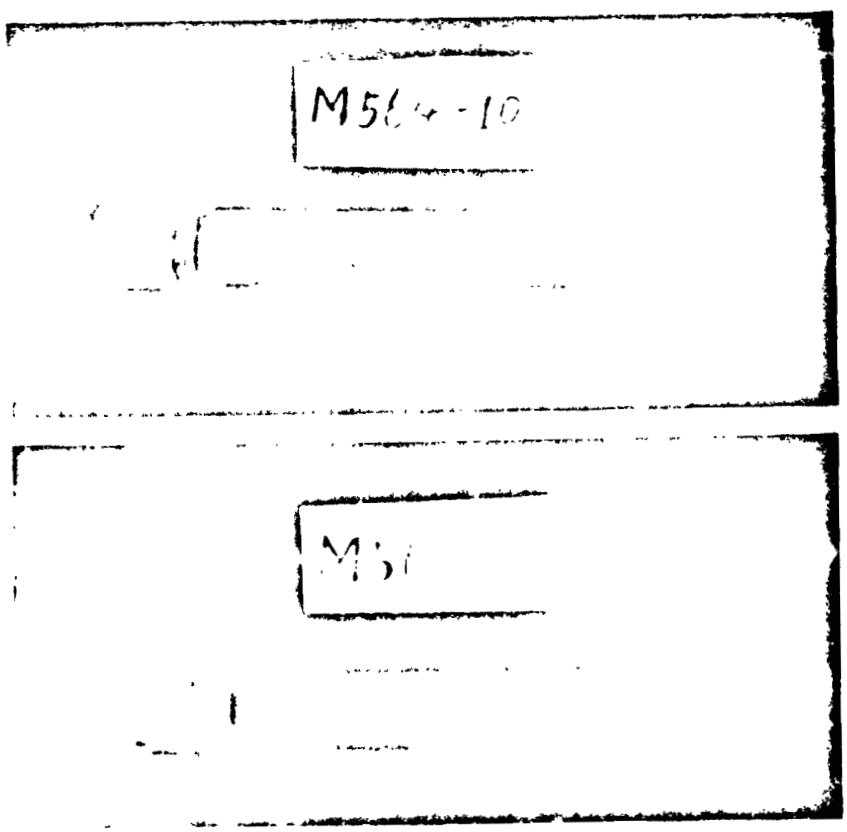

Figure 4. Macro-photograph of NaCℓ-NaF Eutectic, Grown in the Skylab.

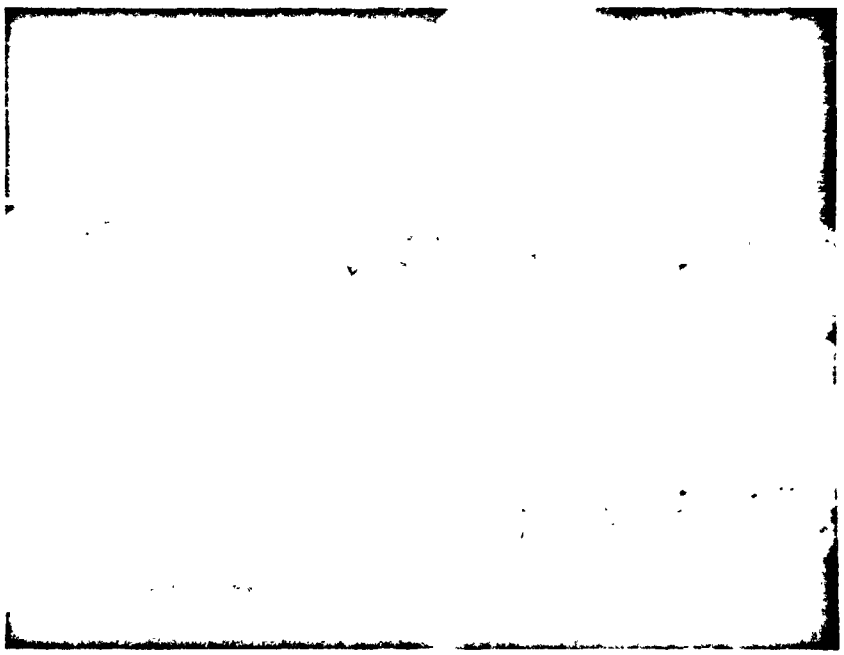

Figure 5. Macrograph Showing the Original Shape of the Solid-Liquid Interface of the Skylab Grown NaCℓ-NaF Eutectic. X6.5

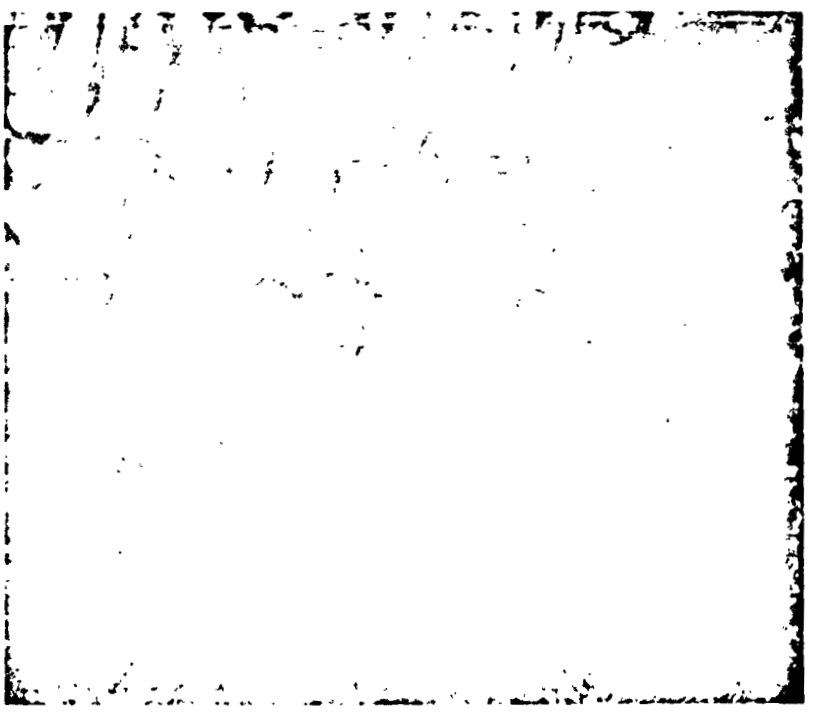

Figure 6. Enlarged Portion at the Original Solid-Liquid Interface. X410

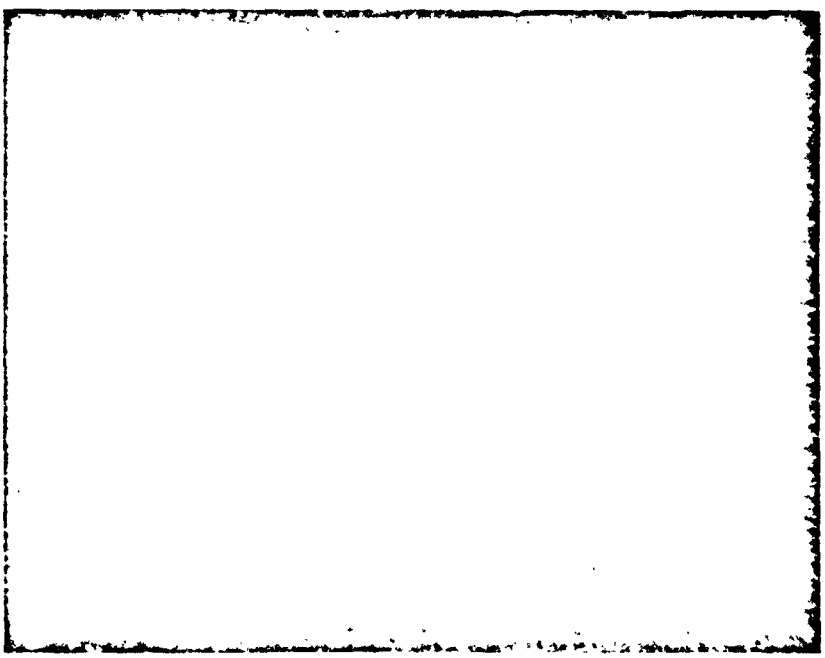

Figure 7. Photomicrographs of a Longitudinal Section of the NaCℓ-NaF Eutectic Showing Continuous NaF Fibers. X135

Figure 8. Photomicrograph of the Transverse Section Showing Shapes of NaF Fibers. X1500

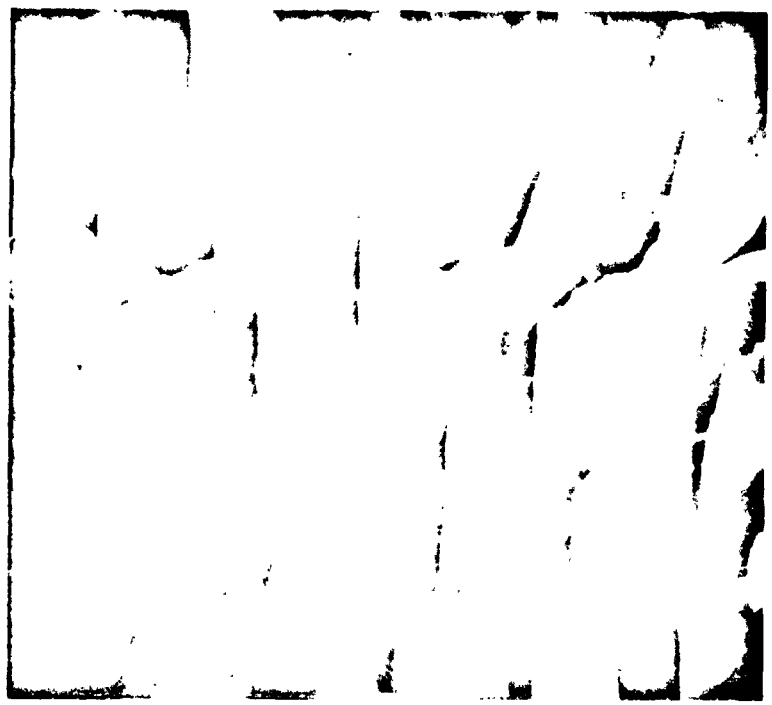

Figure 9a. Scanning Electron Photomicrograph of the Earth-Grown NaF Fibers. X2100

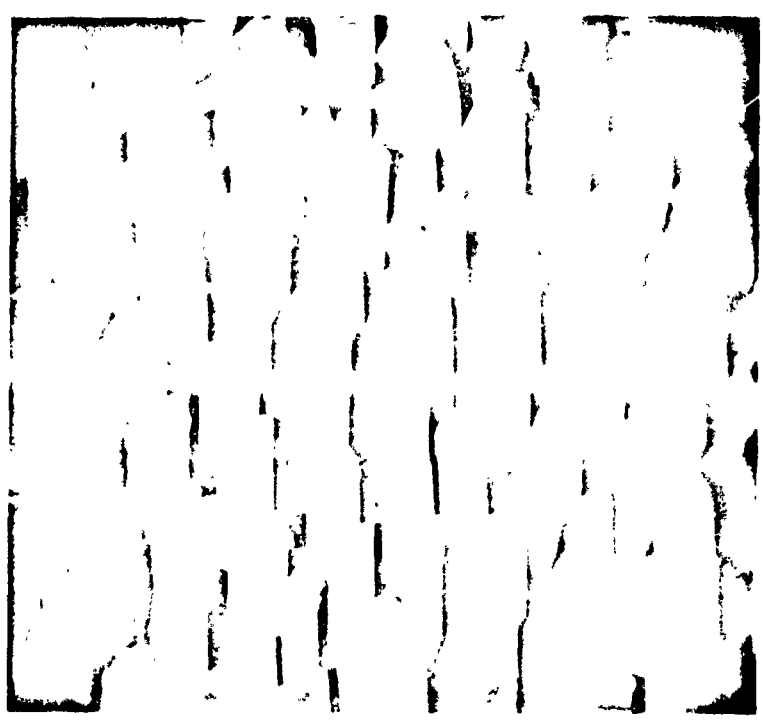

Figure 9b. Scanning Electron Micrograph of the Skylab-Grown NaF Fibers, X3200

direction. This demonstrates that the direction of heat flow was perpendicular to the advancing solid-liquid interface during the solidification process in the Skylab after the interface had moved away from its starting point.

Single-grain eutectic was not produced in the presence of microgravity in space as evidenced in Figure 10 which is a transverse section of sample #10. Many grains are present throughout the whole cross-section. However, the fibers are aligned very regularly parallel to the growth direction.

Evidence supporting this is given in Figure 11a which is a picture taken from sample #6 grown in space. Filtered light from a Bausch & Lomb microscope was directed at the lower end of the sample. Due to good alignment of NaF fibers along the sample axis, light was transmitted from the lower end to and terminated at the melt-back interface which is about 1.4cm away from the upper end of the sample. Light was not transmitted through the unmelted portion of the sample because the fibers did not line up with the sample axis. Note the homogeneity of the sample as revealed in Figure 11a. Figure 11b is a portion of a NaCl-NaF eutectic sample grown vertically on Earth in a prototype furnace (group B) with very little convection current in the melt during growth. Light was completely transmitted from one end to the other, indicating that the NaF fibers are aligned in the direction of the growth axis. However, many striations appeared on the surface of the cylindrical sample, indicating the presence of non-homogeneity in the sample. A non-homogeneous crystal can be transformed to a homogeneous one if it is grown in a space environment with negligible gravity. Figure 11c is a picture taken from a sample grown in an induction furnace at UCLA, (group A). An attempt was made to shine a light at one end of the sample but it did not travel very far because the NaF fibers were not well-aligned in the direction of the light. However, when light was shone on the side of the sample as indicated by the white spot

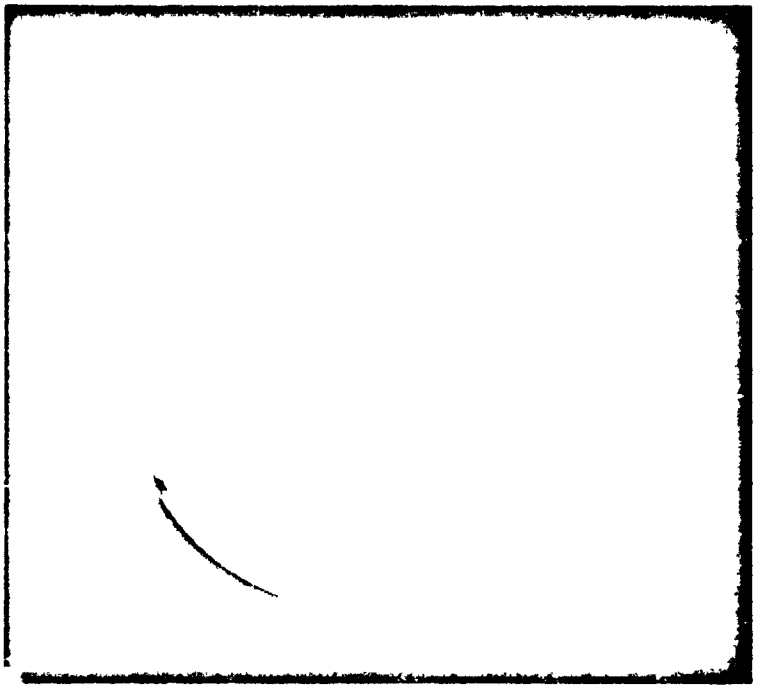

Figure 10. Macrophotograph of the Transverse Section of the NaCℓ-NaF Eutectic, Showing Grains and Subgrains. X9 Sample No. 10

Figure 11. Macrophotographs of Skylab-Grown (a), NASA-Grown (b) and Earth-Grown (c) NaCl-NaF Eutectic.

in Figure 10c, some transmittance of light occurred in the direction perpendicular to the sample axis as well as parallel to the axis, indicating that the fibers, while predominantly parallel to the axis, are also partially perpendicular to it. Banded microstructure was evidenced in Figure 11c in agreement with our original prediction.

4.2 Sodium Fluoride Fibers

Figure 12a is a macrograph of a space-grown ingot that was immersed in methyl alcohol for five weeks to dissolve the NaCl matrix. The surface of the undissolved portion of the ingot is encased with a sheath of NaF fibers. An enlarged portion of the ingot containing the unmelted portion is given in Figure 12b. Notice that, on the right-hand side of the interface, the undissolved portion of the eutectic ingot reveals the presence of striations along the ingot axis. However, the striation directionality was not evident in the unmelted portion of the ingot, indicating that the fibers are short and randomly distributed. Figure 13a proves that the growth of fibers originated at the solid-liquid interface. Figure 13b is a picture of the end cross section of the unmelted portion of the ingot, showing that the short NaF fibers produced on Earth (before the experiment), are perpendicular to the cylindrical surface of the ingot. A macrograph of the lower end of a Skylab-grown ingot after dissolving the NaCl matrix in alcohol is given in Figure 14 which shows that the NaF fibers are indeed continuous. Since the macrograph was taken when the ingot was dried, the NaF fibers appear wavy. Figure 15 is a photograph of a Skylab-grown ingot taken when the NaF fibers were suspended in methyl alcohol. From this figure, it is evident that the individual NaF fibers are fine and straight. When the Earth-grown NaCl-NaF eutectic ingot was immersed in the same solution, NaF fibers could also be extracted from the NaCl matrix. However, the extracted fibers were short and discontinuous

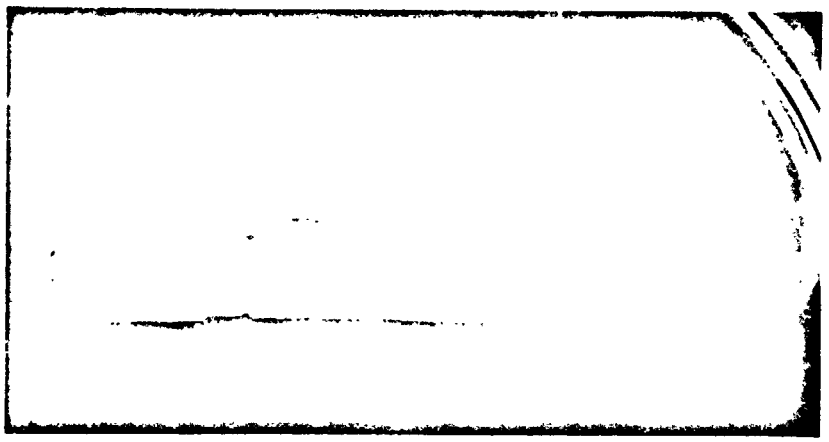

(a)

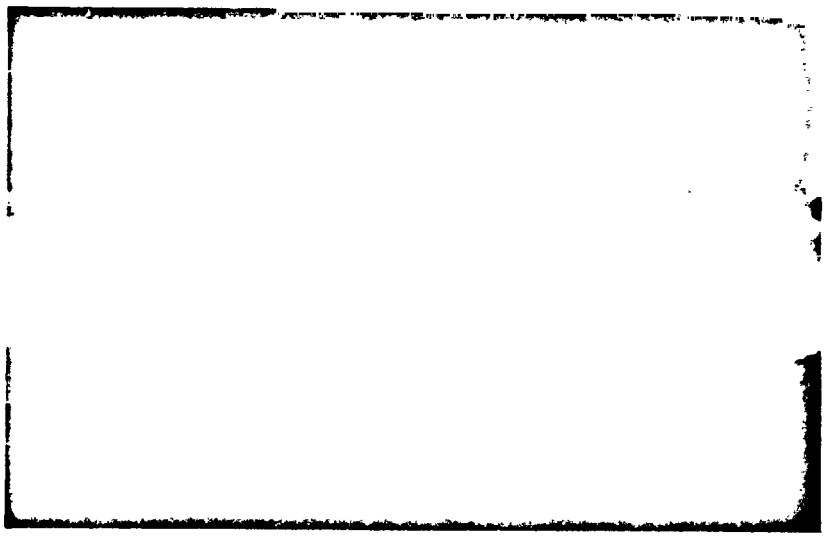

(b)

Figure 12. Skylab-Grown Ingots Encased with Continuous NaF Fibers. (a) X2 and (b) X4.3. Sample No. 11.

Figure 13a. Continuous NaF Fibers Grown Initially from the Solid-Liquid Interface.

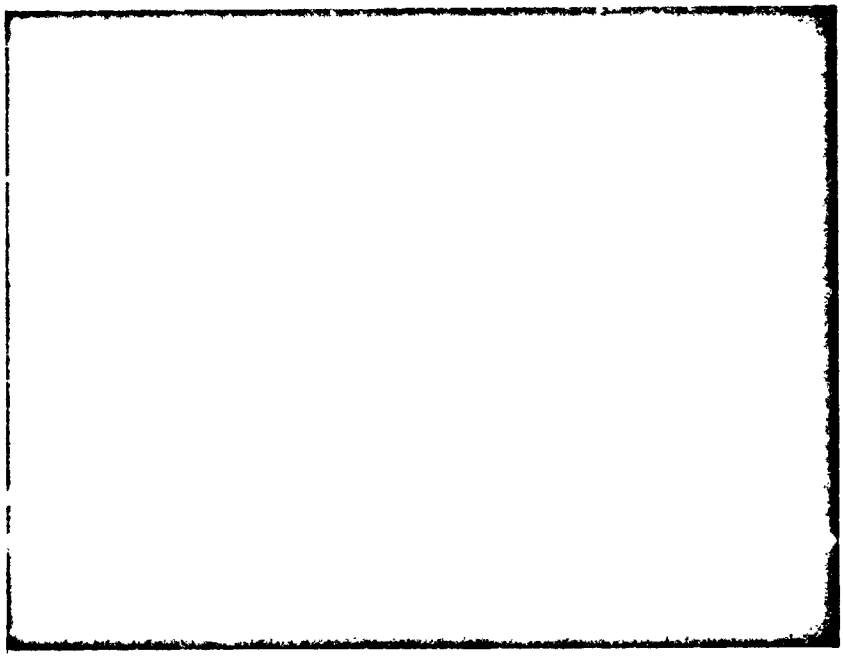

Figure 13b. Discontinuous and Randomly Oriented Fibers of the Earth-Grown Ingot End. X8.6. Sample No. 11.

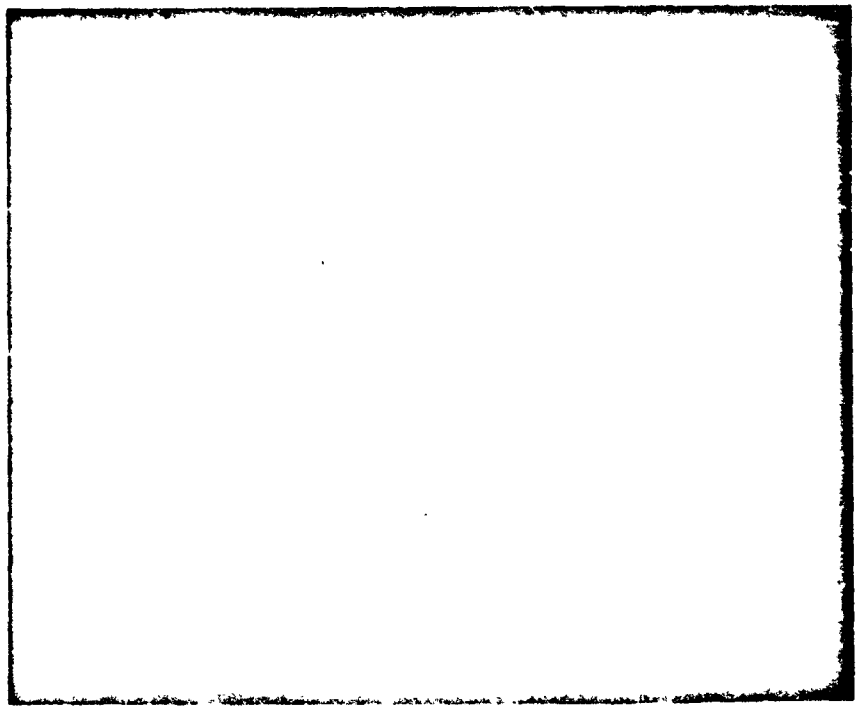

Figure 14. Macrograph of the End of the Skylab-Grown M564-11 Ingot, Showing Continuous NaF Fibers (Picture was Taken After the Ingot was Dried). X8.6

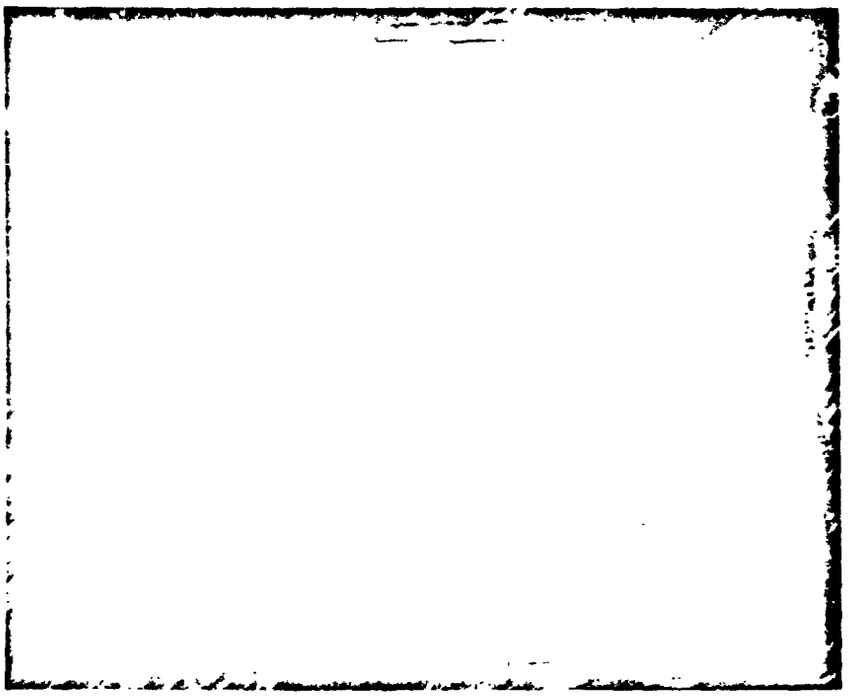

Figure 15. Extracted Continuous NaF Fibers Suspended in Methyl Alcohol. X384 (Skylab Sample No. 11.)

as indicated in Figure 16 in agreement with prediction, (sample from group B). In view of the above analysis, it is concluded that continuous NaF fibers have been produced in space.

4.3 Advancing Solid-Liquid Interface

According to Yue [8], the formation of a tilt boundary in a eutectic mixture is attributed to the presence of an indentation generated at the perturbed solid-liquid interface as predicted by Mullins and Sekerka.[9] This indentation may be reflected in the eutectic solid as a small tilt between the fibers on each side of the indentation and shows up as a tilt boundary with faults of like sign. This is illustrated in Figure 17 which shows a small-angle (15°) tilt boundary (Skylab sample #6). On the basis of this observation, it is tentatively concluded that a microscopically planar advancing solid-liquid interface was not produced in the absence of gravity for the present eutectic, which was not totally pure, (99.96% NaCl and 99.7 % NaF).

4.4 Inter-fiber Spacing

From the thermal data supplied by Westinghouse, we have calculated a range of growth rate varying from 0.5 micron/sec to 4 microns/sec for group B samples. The measured inter-fiber distances in Space-grown and Earth-grown ingots at growth rates around 3.5 micron/sec are listed below:

Interfiber Distance, Microns

Space-Grown	Earth-Grown
5.6 (M564-6)	5.2 (M564-9)
4.8 (M564-10)	4.3 (M564-14)
6.2 (M564-11)	

The average diameter of the fiber is from 2 to 3 microns. These measurements indicate that there is no significant difference in interfiber distance between the Space-grown and the Earth-grown ingots.

Figure 16. NaF Fibers Extracted from Earth-Grown NaCℓ-NaF Eutectic. X7.6

Figure 17. Micrograph of NaCℓ-NaF Eutectic Showing a Small Angle Tilt Boundary. X135

4.5 Image Transmission

Image transmission properties similar to those of fiber optic materials have been obtained by others with an NaCl-NaF eutectic.[10] Since the eutectic in that case had discontinuous NaF fibers, far better results will be obtained if the same eutectic can be produced in space with continuous fibers. Two cylindrical sections 2.5 cm long were cut from Skylab-grown and Earth-grown (group B) samples. Image transmission experiments were made on these two samples. Their results are given in Figure 18. Figure 18a shows that an image was transmitted from a source (a sheet of paper containing the word "Skylab") through the length of the sample, to its surface. The transmitted image has the same dimensions as the source, indicating that the NaF fibers are perpendicular to the plane of the paper. However, the transmitted image is not as clear as the original image of the source indicating that there is a loss through transmission. Some loss is common to all fiber optics materials.[11] A transmitted image was not observed from a sample grown on Earth as evidenced in Figure 18b. This is attributed to the presence of discontinuous and randomly distributed NaF fibers in the NaCl-NaF eutectic produced on Earth.

4.6 Optical Transmittance

Figure 19 is a plot of transmittance vs. wave number k (40×10^2 to 4×10^2 cm^{-1}) for NaCl-NaF eutectics grown at UCLA (group A) and grown in the Skylab (group C). The transverse sections of the eutectic sample were 0.107 in. thick. For the NaCl-NaF eutectic grown at UCLA, where there were convection currents present in the liquid during growth, the transmittance was about 10% over a narrow range of wave numbers, as indicated in Figure 19. When the same eutectic was grown in space, where there were no convection currents in the liquid during growth, the transmittance was increased to 65% over a much

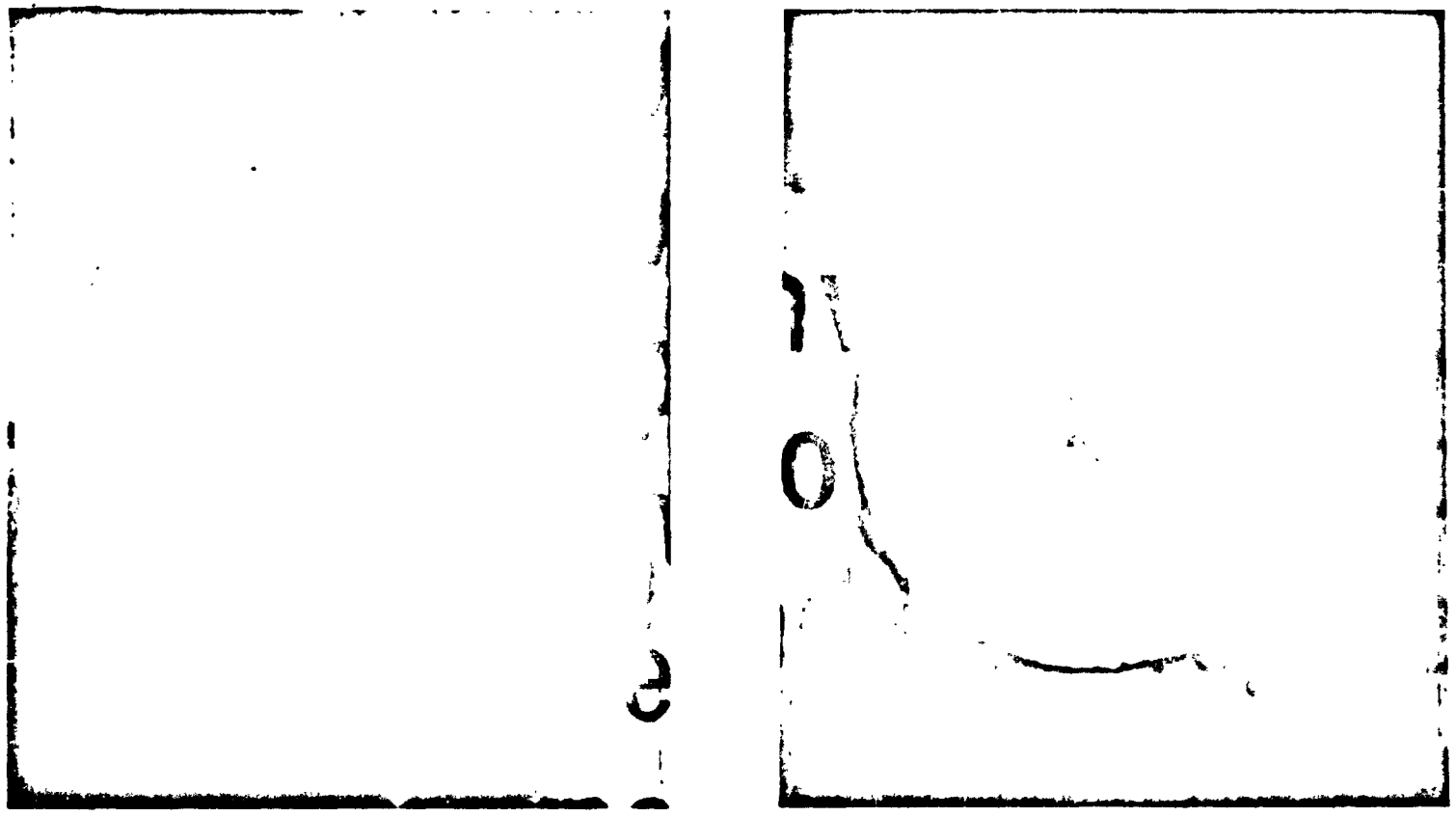

(a) (b)

Figure 18. Image Transmission Macrograph of Skylab-Grown (a) and Earth-Grown (b) NaCℓ-NaF Eutectics. Sample Thickness = 2.5 cm. X8.5

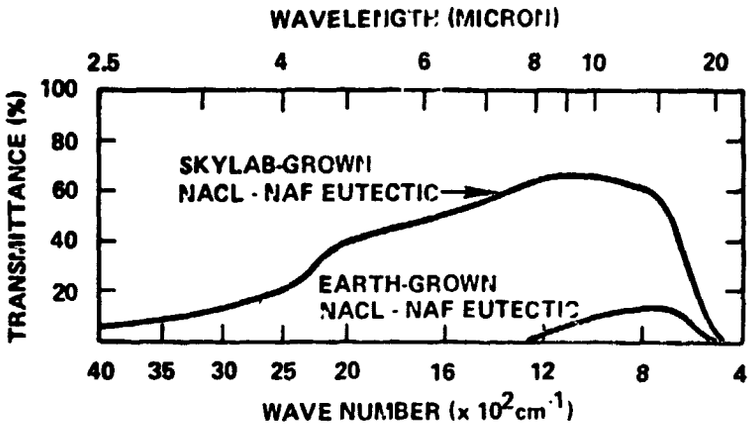

Figure 19. Far infrared transmittance curves for NaCl-NaF eutectics grown on earth and in space. Sample thickness = 0.107 in. (Transverse section)

larger range of wave numbers. This was attributed to the achievement of producing continuous NaF fibers embedded in a continuous NaCl matrix so that the losses due to reflection and refraction of light within the eutectic specimen have been reduced greatly. The shape of the transmission curve for the Skylab-grown NaCl-NaF eutectic is of great interest. At $k > 40 \times 10^2$ cm^{-1}, the transmittance of this eutectic approaches zero. The explanation is that the interfacial atoms at the fiber-matrix interface are mismatched. When incident light is directed at the surface of a eutectic sample, a large fraction of the incident light transmitted through the eutectic sample will be lost due to scattering. This observation is in agreement with the fact that the higher the wave number (or the shorter the wavelength), the higher the loss through scattering.

Figure 20 is a plot of transmittance versus wavelength of a transverse section of a sample vertically-grown on earth (group B) having varying thickness. The results indicate that at a wavelength of 6μ, the transmittance increases from 40% to 70% when the sample thickness was reduced from 0.080 in. to 0.063 in. However, the increase in transmittance is not evident at a wavelength greater than 15μ. Figure 21 shows the effect upon transmittance of etching in alcohol to dissolve the NaCl matrix. It is seen that such short etching produces no change at the long wavelength, and minor changes at the short wavelength end of the range (5 to 20 microns).

Figures 22a and 22b show the effect of thickness on the transmittance perpendicular to a longitudinal section of a UCLA-grown sample (group A), using polarized light with electric field parallel and perpendicular to the fiber axes respectively. Figures 23a, 23b and 24 show the same curves for Earth-grown samples (group B). In this group, sample #9 was vertically grown, but sample #3 was horizontally grown. Fibers of sample #3 were not aligned

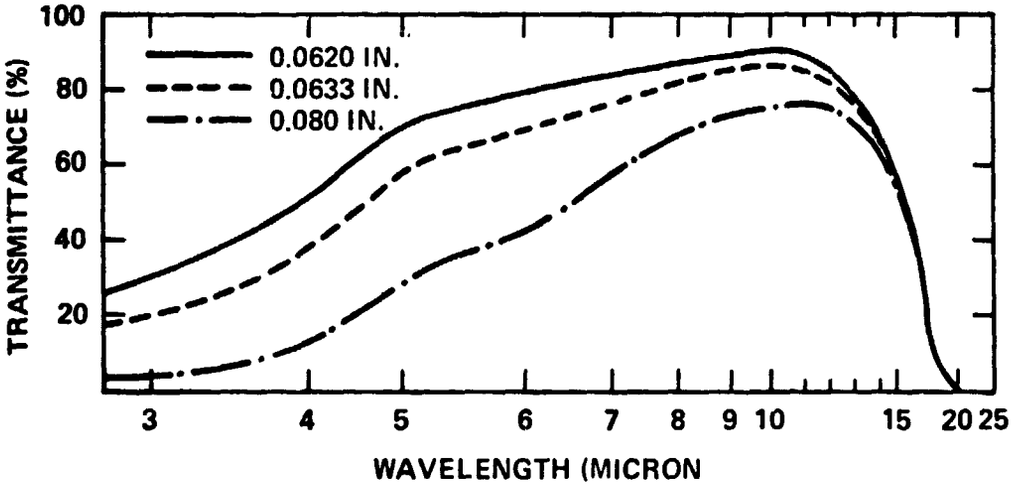

Fig. 20. Far infrared transmittance curves of a transverse section of vertically grown eutectic (M564-9) of varying thicknesses.

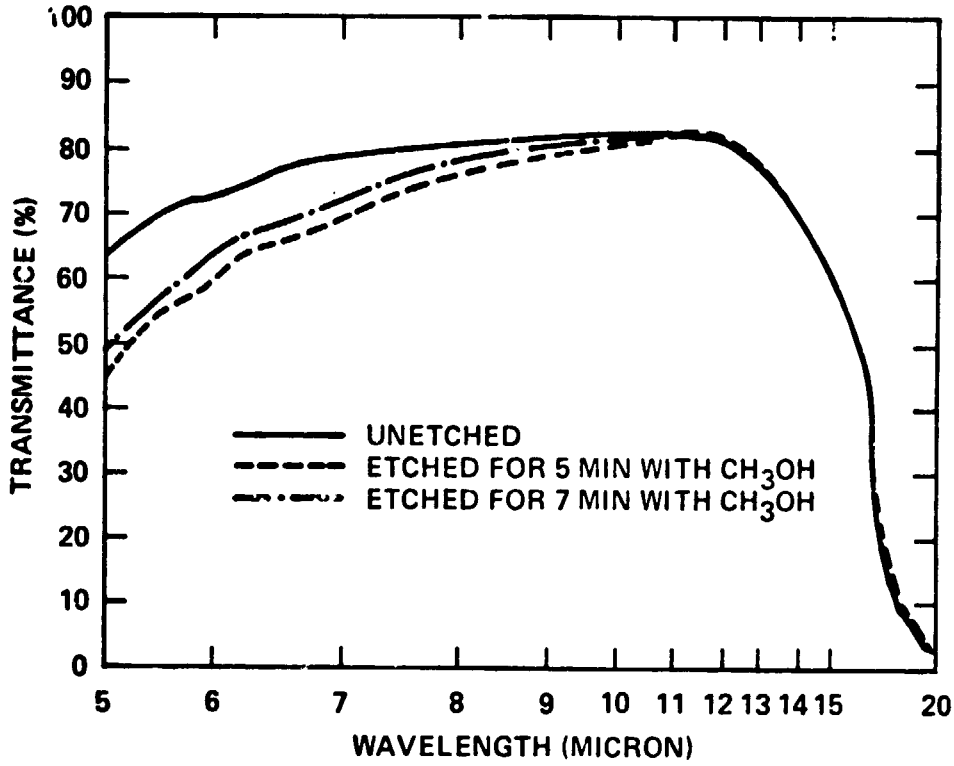

Figure 21. Etching effect on far infrared transmittance curves of a transverse section of vertically grown NaCl-NaF eutectic (M564-9). Thickness ≈ 0.0382 in.

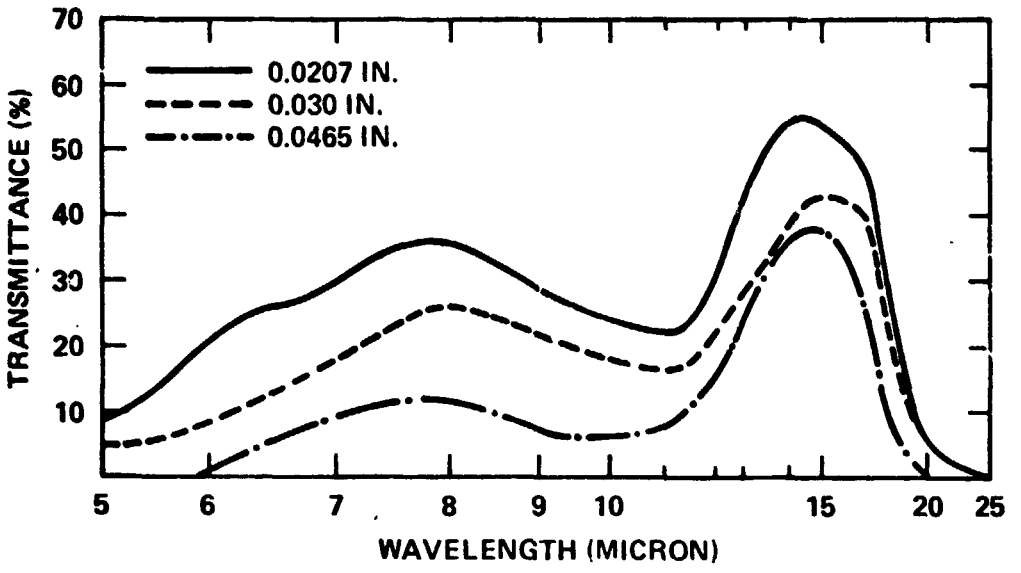

Figure 22a. Far infrared transmittance curves of a longitudinal section of UCLA-grown NaCl-NaF eutectic of varying thicknesses. $\vec{E} \perp$ to fiber axis.

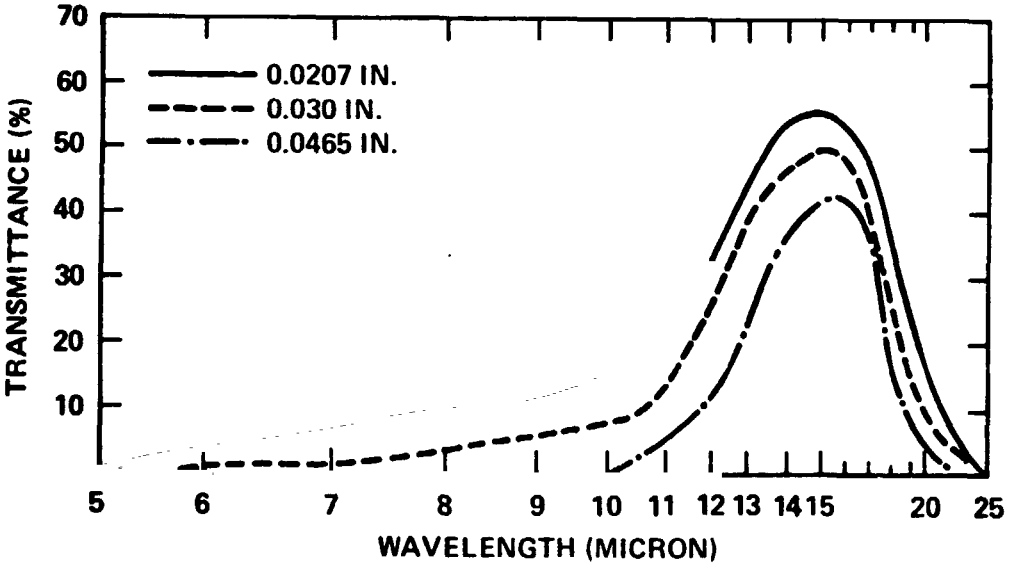

Figure 22b. Far infrared transmittance curves of a longitudinal section of UCLA-grown NaCl-NaF eutectic of varying thicknesses. $\vec{E}_{\parallel}$ fiber axes

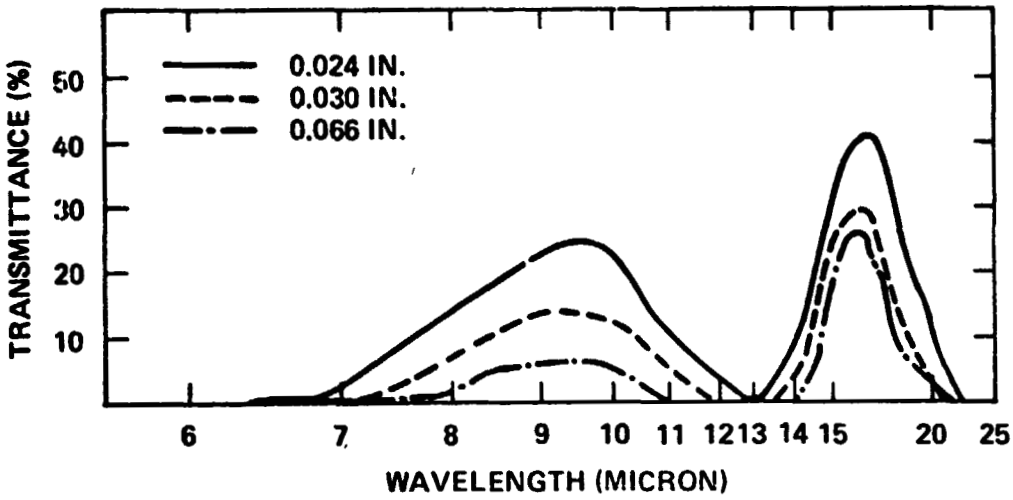

Figure 23a. Far infrared transmittance curves of a longitudinal section of vertically grown NaCl-NaF eutectic (M564-9) of varying thicknesses. $\vec{E}$! fiber axis.

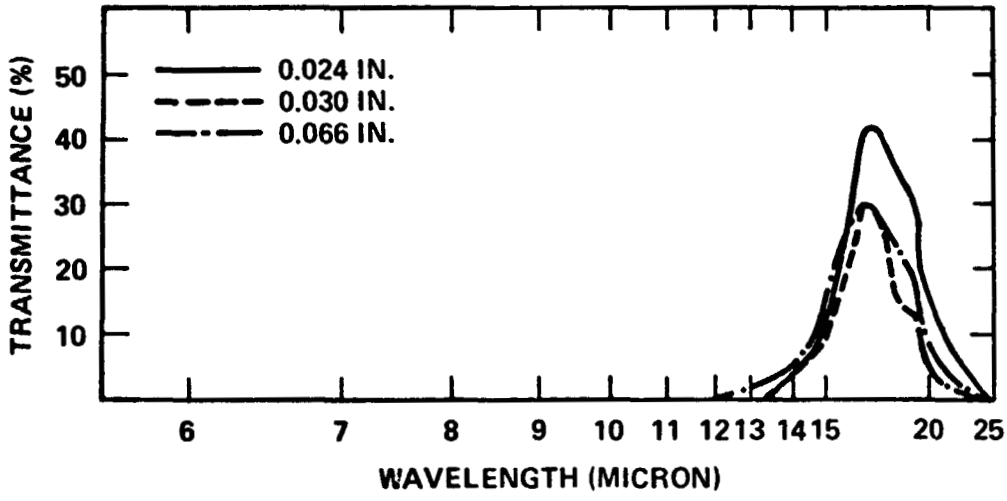

Figure 23b. Far infrared transmittance curves of a longitudinal section of vertically grown NaCl-NaF eutectic (M564-9) of varying thicknesses. $\vec{E}_{\parallel}$ fiber axis.

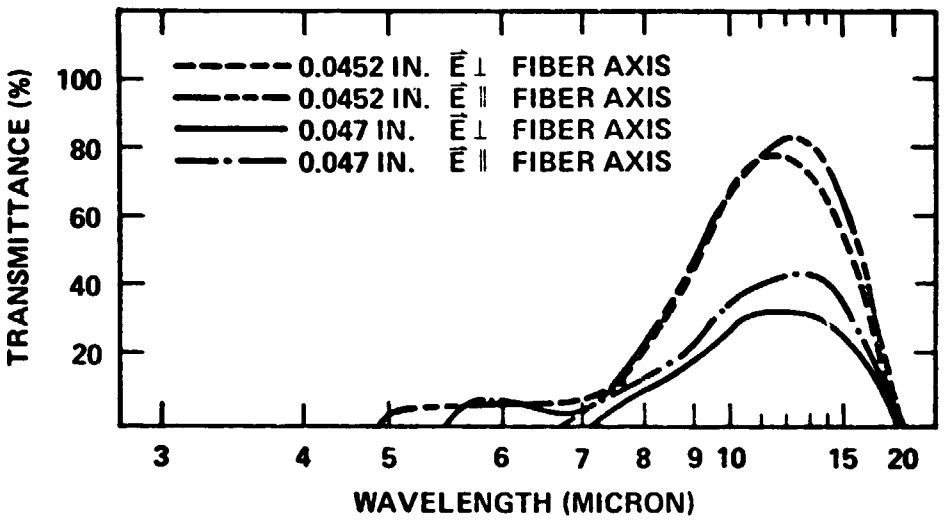

Figure 24. Far infrared transmittance curves of a longitudinal section of horizontally-grown NaCl-NaF eutectic (M564-3) of varying thicknesses.

due to the strong convection current during the growth. Hence the transmittance curve of a longitudinal section of sample #3 shows almost no transmittance for wavelength less than 7μ. Figures 25a, 25b, 26a and 26b show the transmittance curves of longitudinal sections of Space-grown samples (group C).

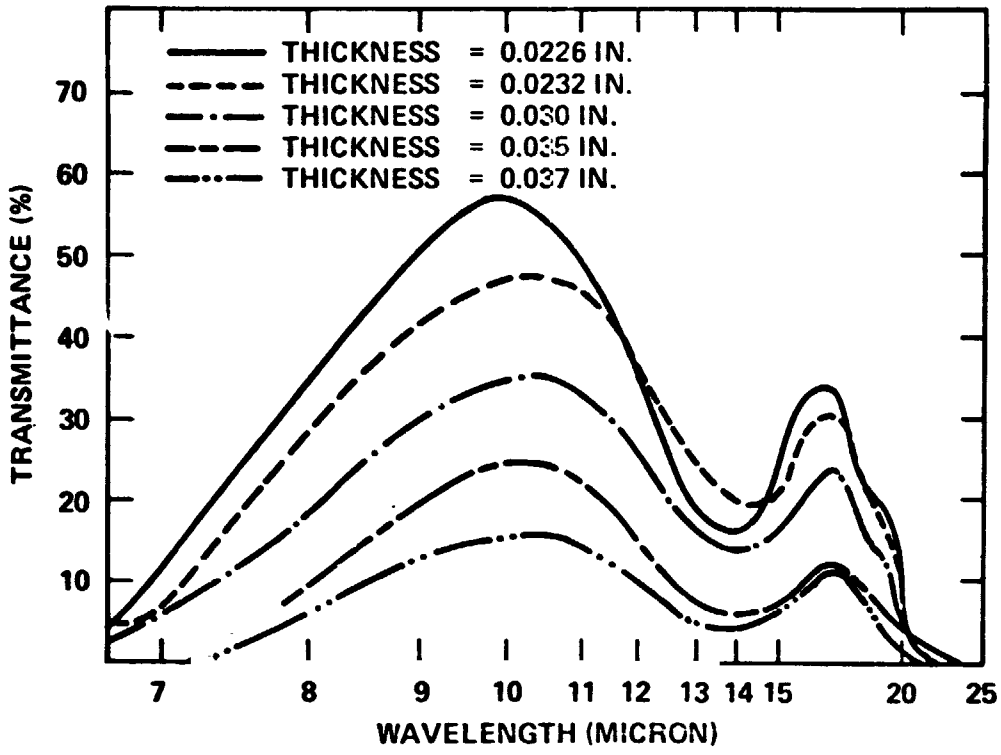

Figure 25a. Far infrared transmittance curves of a longitudinal section of NaCl-NaF eutectic (M564-6) of varying thicknesses. $\vec{E} \perp$ fiber axis.

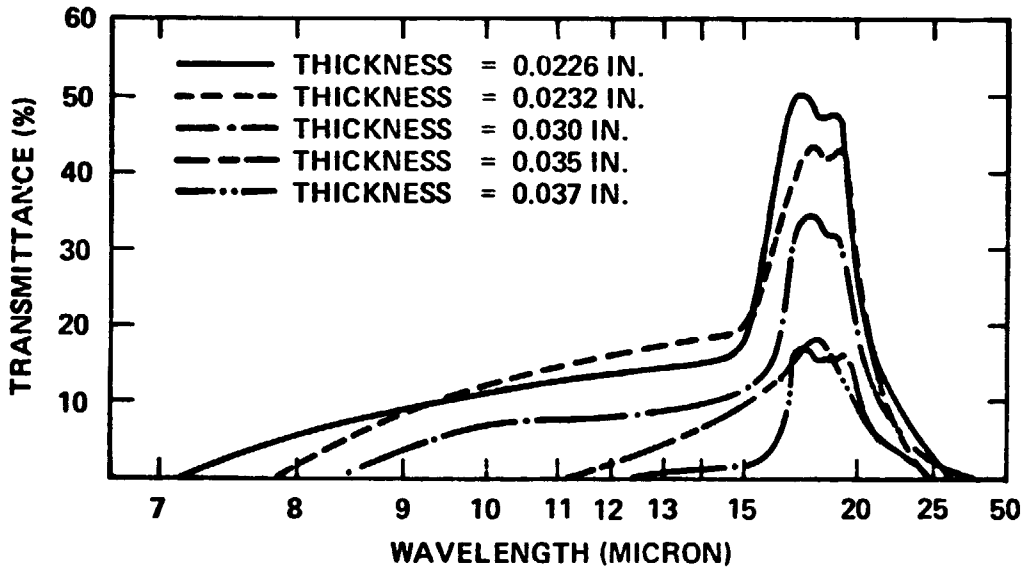

Figure 25b. Far infrared transmittance curves of a longitudinal section of NaCl-NaF eutectic (M564-6) of varying thicknesses. $\vec{E}_{\parallel}$ fiber axis.

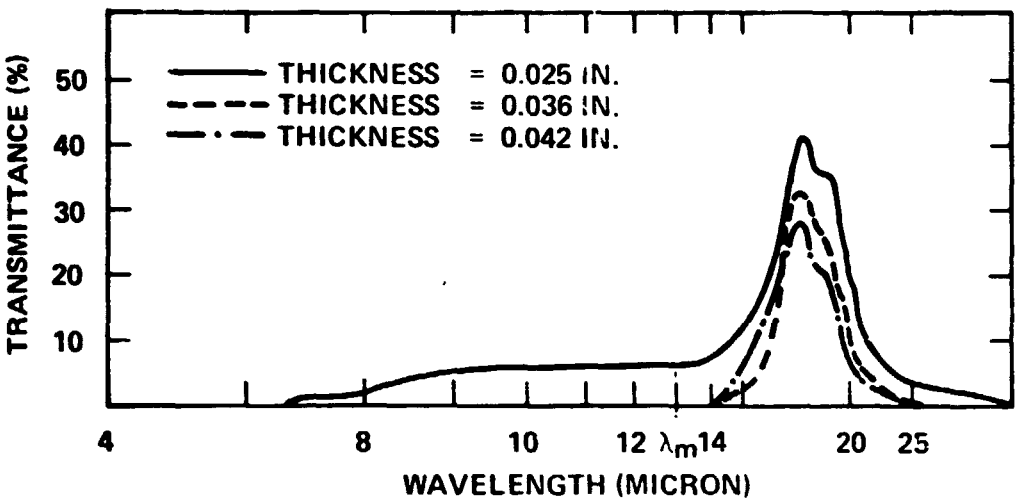

Figure 26a. Far infrared transmittance curves of a longitudinal section of NaCl-NaF eutectic. (M564-10) of varying thicknesses. $\vec{E} \parallel$ fiber axis.

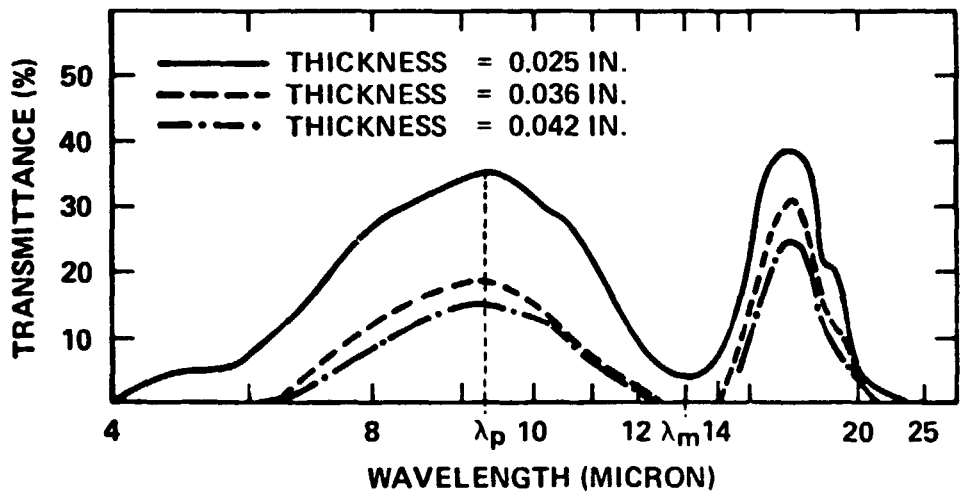

Figure 26b. Far infrared transmittance curves of a longitudinal section of NaCl-NaF eutectic. (M564-10) of varying thicknesses. $\vec{E} \perp$ fiber axis.

Section 5

DISCUSSION

5.1 NaF Fibers

In a zero-gravity environment, there is no gravity-driven convection current in the liquid during solidification and there is no difficulty in mixing two liquid phases of different densities. Furthermore, vibration levels in the spacecraft will be far lower than those on Earth. Consequently, a homogeneous eutectic mixture consisting of continuous fibers can be produced in a space environment, and microstructure sensitive to convection currents and vibration can develop undisturbed. Accordingly, the success in producing continuous NaF fibers as evidenced in Figures 12 and 15 is mainly due to the absence of convection current in the melt during resolidification in space.

5.2 Optical Transmittance

Pure sodium chloride and sodium fluoride crystals, as is known from previous work, have approximately 95% transmittance per cm of thickness up to 15 and 9 microns respectively in the far infrared wavelength region. These curves are shown for comparison at the right of Figure 27. Beyond these ranges of wavelengths, these crystals have zero transmittance due to the optical modes of lattice vibration of ionic crystals. Figure 27 also shows a set of transmittance versus wavelength curves of Skylab-grown (M564-6) and Earth-grown (UCLA) fiberlike NaCl-NaF eutectics. If a thin piece of either one of these eutectics is cut along its fiber axis (longitudinal section) as illustrated in Figure 28, and is measured from 4 to 25 microns (μ) wavelength with an infrared spectrometer, typical transmittance versus wavelength curves with polarized beam parallel and perpendicular to fiber axes are given in Figures 26a and 26b, respectively. For the electric field parallel to fiber axes the transmittance is near zero over a range of wavelength less than λ_m (13 μ),

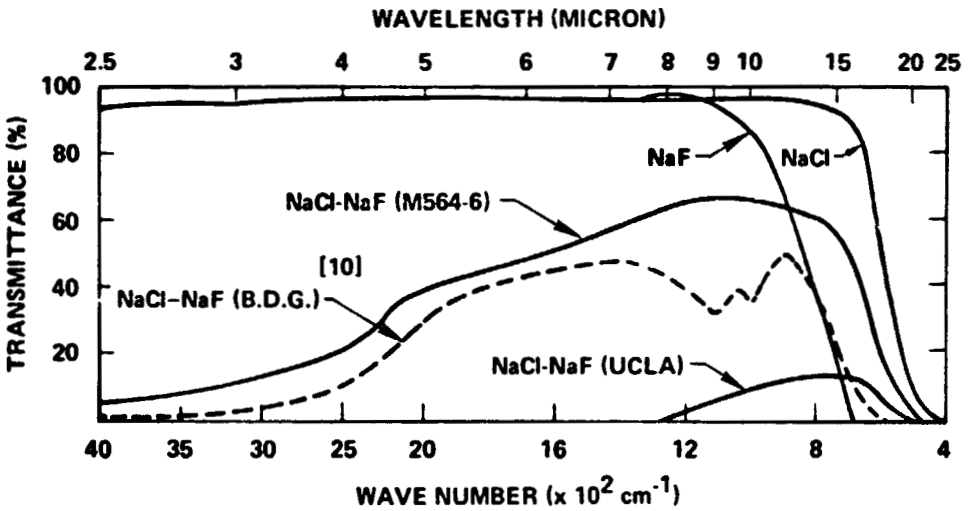

Figure 27. Far infrared transmission curve of transverse sections of NaCl-NaF [10] eutectics grown on earth and in space. Sample thickness = 0.107 in.

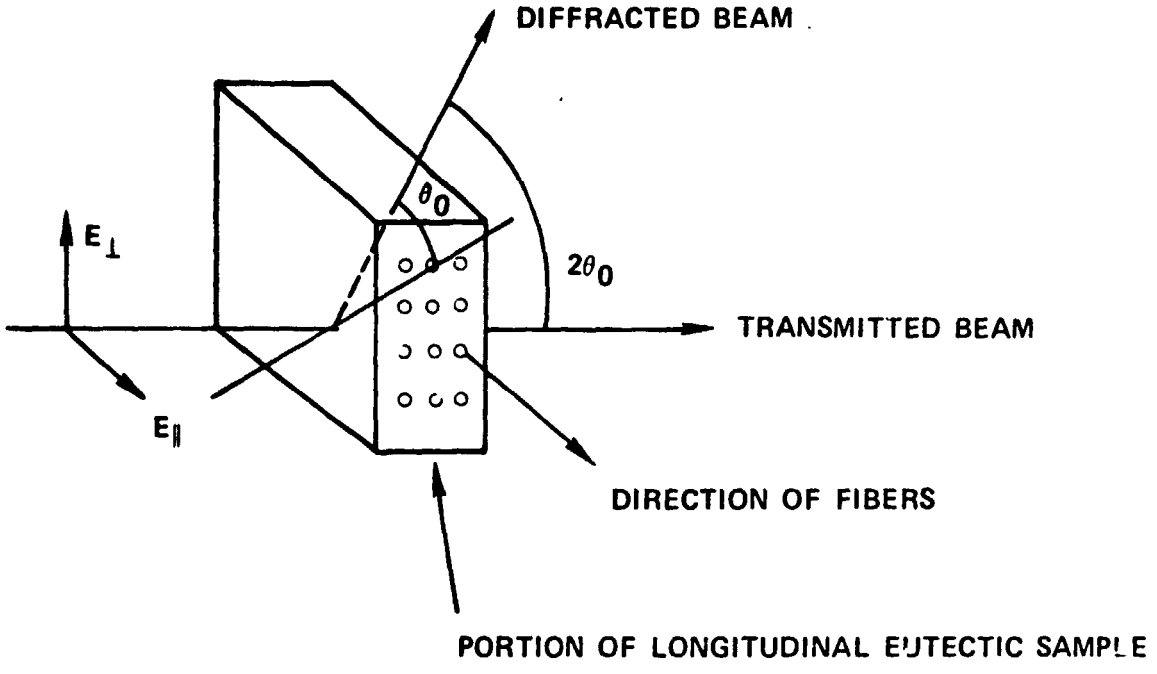

Figure 28. Diagram illustrating quantities discussed in analyzing scattering measurements, for transmission through a longitudinal sample section.

a maximum wavelength. When the electric field is perpendicular to the fiber axes, the percentage of transmittance increases over a range of wavelengths less than λ_m and reaches a maximum value at a wavelength of 9.2 μ, which is designated λ_p, a peak wavelength, as indicated in Figure 26b. Since a thin NaCl-NaF eutectic sheet has these characteristics, it can be used as a polarizer and a modulator. It can switch on and off the light at a specified wavelength when the electric field is rotating. An explanation is advanced to account for this phenomenon in terms of two-dimensional Bragg Scattering and the polarization effect of Rayleigh scattering.

5.3 Theoretical Consideration of Optical Transmittance

We consider now transmittance through a longitudinal section, i.e., beam perpendicular to the fibers, as shown in Figure 28. Since the fiberlike microstructure of a transverse section of NaCl-NaF eutectic ingot has a hexagonal periodicity[12] and the average fiber diameter and interfiber distance are 2 and 6 microns, respectively which are less than the wavelength that we are interested in, it can be assumed that the light is coherent and that it propagates through a continuous NaCl matrix and is scattered by the NaF fibers. In other words, only the index of refraction of NaCl should be involved, not the effective index of refraction of the NaCl-NaF eutectic as suggested by Sievers.[13] This hypothesis is reasonable and consistent because scattering by NaF fibers is taking place for wavelengths greater than the average diameter of NaF fibers. If we assume that NaF fibers are transmitting the light perpendicular to the fiber, from one side to the other, then the high value of the number of fiber-matrix interfaces per unit volume would give essentially zero transmittance for a range of wavelength greater than λ_m. According to Figures 26a and 26b, this is not the case, because a significant hump appears in transmission below this wavelength. Assume,

then, that light is transmitted through the NaCl matrix but scattered by the fibers. Whenever Bragg's Law is satisfied, the percentage of transmittance decreases due to the constructive reflection loss, since such diffracted beams will leave the sample at other angles and will not be seen in measurement of the transmitted beam at $\theta = 0°$. In our consideration we use the index of refraction of NaCl, $n_{NaCl}(\lambda)$, instead of using the effective index of refraction,[2] $\bar{n}(\lambda)$. Accordingly, Bragg's Law for a two dimensional hexagonal lattice is expressed as

$$\lambda = \sqrt{\frac{3}{h^2+hk+k^2}}\, n_{NaCl}(\lambda)\, \bar{d}\, \sin\theta \qquad (1)$$

and the maximum wavelength which satisfies Bragg's Law is

$$\lambda_m = \sqrt{3}\ n_{NaCl}(\lambda_m)\, \bar{d}, \qquad \text{for } h=1,\ k=0,\ \theta(\text{interior angle}) = 90° \qquad (2)$$

where λ and λ_m are the wavelengths (in free space) as defined previously, h and k are Miller indices, θ is the Bragg angle inside the crystals, d is the average interfiber distance and $n_{NaCl}(\lambda_m)$ is the index of refraction of NaCl at a specific wavelength. Since light can still be transmitted through the NaCl-NaF eutectic mixture at a far infrared wavelength greater than λ_m, as indicated in Figures 26a and 26b, its cut-off transmittance is related to the intrinsic cut-off value (25 μ) of the NaCl crystal, not that (15 μ) of the NaF fibers, (see Figure 27). This additional evidence supports our assumption that light is transmitted through the NaCl matrix.

It is well known[15,16] that in scattering from isolated scattering points, when the scattering angle 2θ is 90°, (here θ is the exterior angle), the scattered wave is polarized, i.e., there is no wave with an electric field parallel to the scattering plane which contains incoming and outgoing rays. In other words, the reciprocal lattice point of this plane is missing at this

specific wavelength with a 90° scattering angle in an Ewald construction. We propose that this same effect explains the present scattering from the NaF fibers. Then for our case, for the electric field perpendicular to the fibers, there can be no beam leaving at 90° due to such constructive reflection; hence the transmitted beam will be a maximum. The transmittance should then have a peak at a wavelength, λ_p, when θ for the reflected wave is 45°, i.e.,

$$\lambda_p = \sqrt{\frac{3}{h^2+hk+k^2}}\; n_{NaCl}(\lambda_p)\bar{d}\,\sin 45° \qquad (3)$$

The experimental data of $\frac{\lambda}{n_{NaCl}(\lambda)}$ and $\frac{\lambda_p}{n_{NaCl}(\lambda_p)\sin 45°}$ versus λ were plotted in Figure 29 which contains two curves. Since the same scattering plane diffracts λ_m and λ_p at 0° and 90° scattering angles, respectively, then we should expect to find

$$\frac{\lambda_p}{n_{NaCl}(\lambda_p)\,\sin 45°} = \frac{\lambda_m}{n_{NaCl}(\lambda_m)}. \qquad (4)$$

A horizontal line, drawn crossing these two curves, yields values of λ and λ_m on the abscissa as indicated in Figure 29. Different lines should yield values matching the data at different values of $\bar{d}$.

The Ewald construction in a reciprocal space of a two-dimensional hexagonal lattice can demonstrate the conditions that the Bragg's Law of reflection is satisfied for wavelengths, λ_m, Figure 30a, and λ_p, Figure 30b, respectively. The radius of an Ewald circle ($n_{NaCl}(\lambda)$) varies with wavelength. The maximum wavelength, λ_m, satisfies the Bragg's Law of reflection with the smallest possible radius of Ewald Circle (Figure 30a). A 90° scattering angle in an Ewald construction as shown in Figure 30b gives a radius of

$$\frac{1}{\sqrt{3}\,\bar{d}\,\sin 45°}$$

which corresponds to a peak wavelength, λ_p.

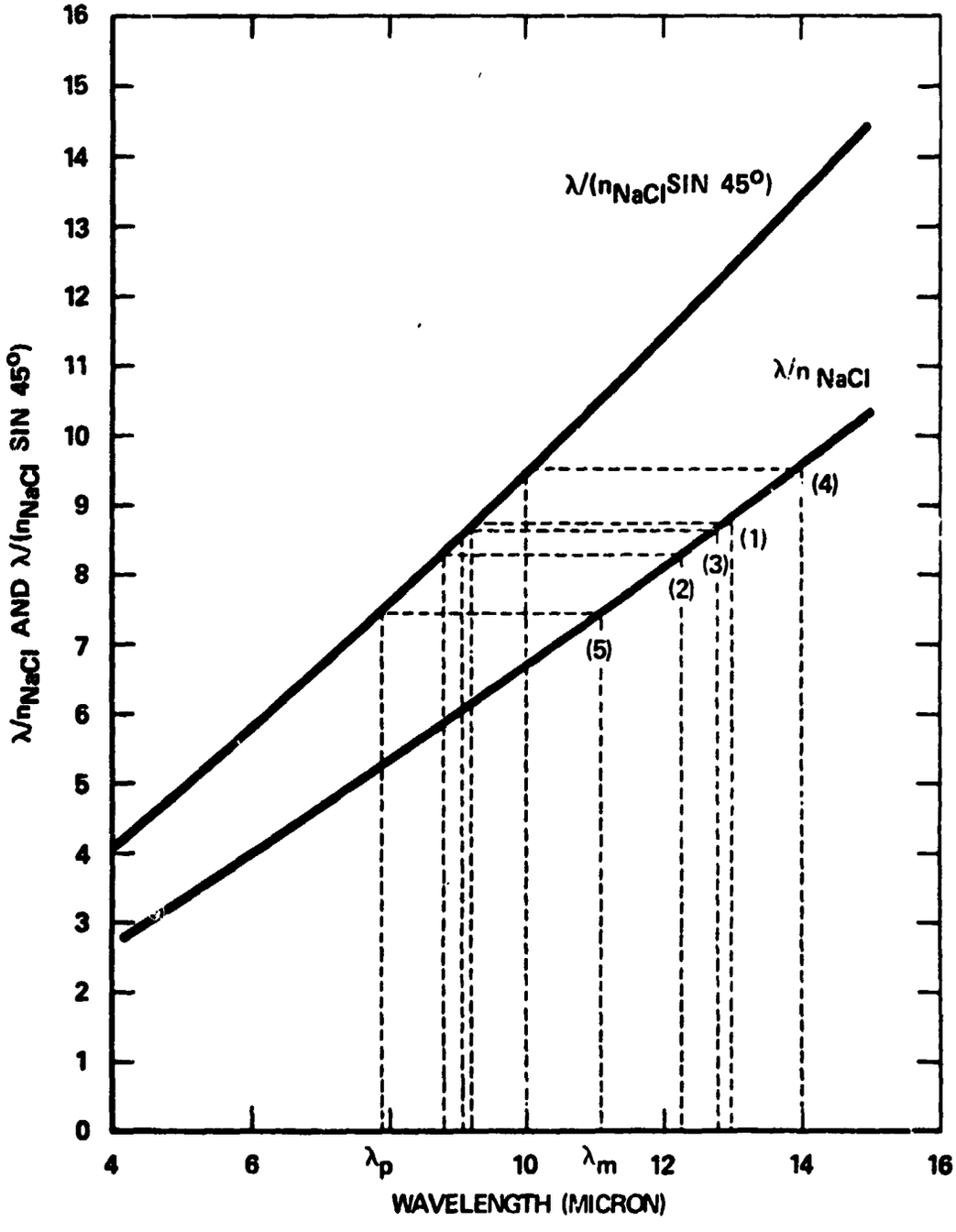

Figure 29. Variation of λ/n_{NaCl} and $\lambda/(n_{NaCl}$ sin 45°) with wavelength of sodium chloride.

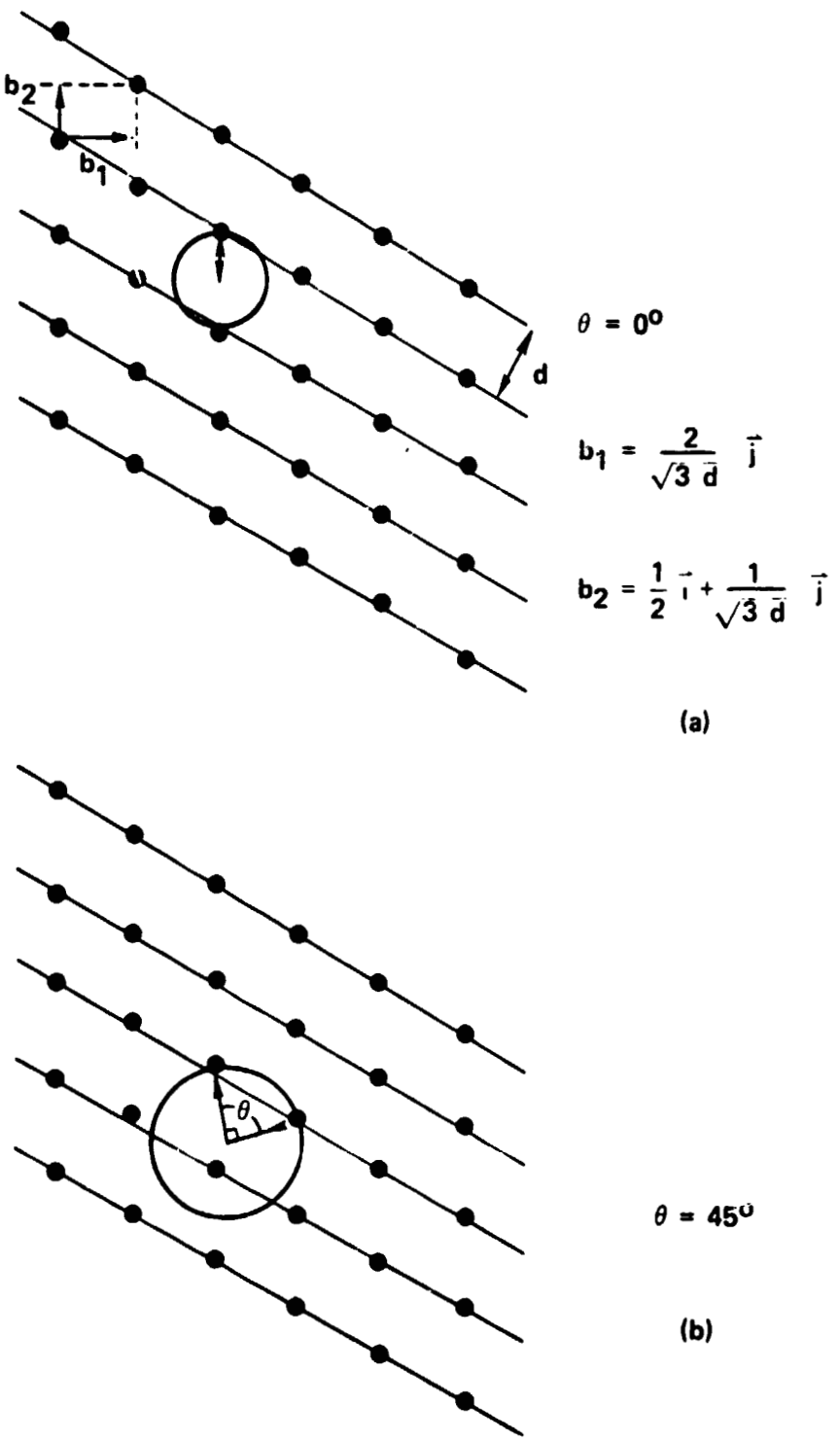

Figure 30. Ewald Circle. (a) Radius is $N_{NaCl\ (\lambda_m)}/\lambda m$ or $1/\sqrt{3}\ d$ and (b) radius is $N_{NaCl(\lambda_p)}/\lambda p$ or $1/(\sqrt{3}\ d \sin\theta)$.

By knowing the experimental values of λ_m, the values of λ_p and the theoretically calculated interfiber spacings, $\bar{d}$ can be predicted from Figure 30 or, given λ_p, we can predict the values of λ_m and $\bar{d}$. This approach can be applied to any of the eutectic systems as long as the index of refraction of the matrix $n(\lambda)$ is known over a range of wavelengths of interest.

Our experimental data of λ_m, λ_p and $\bar{d}$ and those of Sievers[13] are listed in Table 1. Both the theoretically calculated λ_p and $\bar{d}$ are in excellent agreement with the experimentally determined values, indicating that our new approach for predicting λ_p and $\bar{d}$ is reasonably sound and justified.

TABLE I

Interfiber Spacings, Maximum Wavelength and Peak Wavelength for Bragg Scattering

	λ_m (microns)	λ_p (microns)		$\bar{d}$ (microns)	
	Measured	Measured	Calculated	Measured	Calculated
Present data (1)	13	9.2	9.2	5.10	5.00
Present data (2)	12	8.4	8.5	4.74	4.80
Sievers data (3)	14	10.0	9.9	5.93	5.80
Present data	14	10.0	10.0	5.60	5.51
Sievers data (4)	11	7.8	7.8	4.35	4.50
Present data	11	7.9	7.9	4.50	4.30

Since our proposed explanation for the peak in transmission at λ_p (for E $\perp$ to fibers) depends upon fiber spacing, $\bar{d}$, the breadth of the experimental peak is presumably due to the range of values of d in the sample. We propose, therefore, that the more uniform the spacing $\bar{d}$, the sharper will be the experimental transmission peak. Hence, one measurement of this peak should serve to define the homogeneity of fiber spacing in the sample.

Section 6

CONCLUSIONS

The following conclusions can be drawn from this report:

1. Continuous NaF fibers, regularly arranged in a NaCl matrix, have been produced in a space environment.

2. Larger transmittance over a wider wavelength and better image transmission were obtained from the space-grown materials.

3. A new concept has been proposed to predict λ_m, the maximum wavelength, and λ_p, the peak wavelength, using the solidification data.

Section 7

RECOMMENDATIONS

1. To design decanting experiments to study the interface morphology in the scientific laboratory to be used in the early flights of the Space Shuttle.

2. To etch out NaF fibers from the NaCl matrix for the study of multiple channel electron intensifiers.

3. To make extensive study on the composition of NaF and NaCl phases using electron microprobe.

Section 8

REFERENCES

1. A.S. Yue and J.B. Clark: Trans. TMS-AIME, 1961.
2. F.D. Lemkey and E.R. Thompson: Met. Trans., 1971, Vol. 2, p. 1537.
3. A.S. Yue: Trans. TMS-AIME, 1962, Vol. 224, p. 1010.
4. F.W. Crossman and A.S. Yue: Met. Trans., 1971, Vol. e, p. 1545.
5. R.W. Kraff and D.L. Albright: Trans. TMS-AIME, 1961, Vol. 221, p. 95.
6. H. Weiss: Met. Trans., 1971, Vol. 2, p. 1513.
7. R. Seidensticker: "Third Space Processing Symposium," April 30-May 1, 1974, Marshall Space Flight Center, Alabama.
8. A.S. Yue, "Lamellar Tilt Boundary of Mg-32 Wt Pct Al Eutectic," Trans. TMS-AIME, Vol. 230, 1964, p. 39-44.
9. W.W. Mullins and R.F. Sekerka, "Stability of a Planar Interface During Solidification of Dilute Binary Alloys," Journal of Applied Physics, Vol. 35, 1964, p. 444-452.
10. J.A. Batt, F.C. Douglas, and F.S. Galasso, "Optical Properties of Unidirectionally Solidified NaF-NaCl Eutectic," Ceramic Bulletin, Vol. 48, 1969, p. 622-626.
11. D.N. Payne and W.A. Gambling: Opto-electronics, 5, 297 (1973).
12. A.S. Yue and J.G. Yu: Thermophysics and Heat Transfer Conference, AIAA/ASME, July 15-17, 1974, AIAA Paper No. 74-646.
13. A.J. Sievers: Proceedings of the Conference on In-Situ Composites, National Academy of Science - National Academy of Engineering, Washington, D.C., 129 (1973).
14. W.A. Bragg and A.B. Pippard: Acta Crystallography, 6, 865 (1953).
15. F.A. Jenkins and H.E. White: "Fundamental of Optics," McGraw-Hill (1957).
16. B.D. Cullity, Elements of X-Ray Diffraction, Addison Wesley, 1967.